The Meteoritical Society

Meteoritics & Planetary Science 45, Nr 9, 1429–1445 (2010)
doi: 10.1111/j.1945-5100.2010.01118.x

The Whitecourt meteorite impact crater, Alberta, Canada

Randolf S. KOFMAN, Christopher D. K. HERD*, and Duane G. FROESE

Earth and Atmospheric Sciences, University of Alberta, Edmonton, Alberta T6G 2E3, Canada
*Corresponding author. E-mail: herd@ualberta.ca

(Received 08 April 2010; revision accepted 27 July 2010)

We dedicate this paper to the memory of Sonny Stevens, without whom this remarkable crater would have continued in obscurity.

Abstract–The <1,100 yr old Whitecourt meteorite impact crater, located south of Whitecourt, Alberta, Canada, is a well-preserved bowl-shaped structure having a depth and diameter of approximately 6 and 36 m, respectively. There are fewer than a dozen known terrestrial sites of similar size and age. Unlike most of these sites, however, the Whitecourt crater contains nearly all of the features associated with small impact craters including meteorites, ejecta blanket, observable transient crater boundary, raised rim, and associated shock indicators. This study indicates that the crater formed from the impact of an approximately 1 m diameter type IIIAB iron meteoroid traveling east-northeast at less than approximately 10 km s^{-1}, striking the surface at an angle between 40° and 55° to horizontal. It appears that the main mass survived atmospheric transit relatively intact, with fragmentation and partial melting during impact. Most meteoritic material has a jagged, shrapnel-like morphology and is distributed downrange of the crater.

INTRODUCTION

The investigation of the broad distribution of crater sizes in the terrestrial impact record has vastly improved understanding of these near instantaneous high-energy events. Investigation of impact events, ranging from meter-sized penetration craters to multikilometer hypervelocity impact basins, may present investigators with a number of site-specific challenges, the level of preservation often representing the most significant. In smaller, and generally younger structures, this may be the result of processes ranging from erosion to anthropogenic activity. Examples include the Morasko (e.g., Stankowski 2001), Campo del Cielo (Cassidy et al. 1965), Carancas (Brown et al. 2008), Sikhote Alin (e.g., Krinov 1966) and Haviland (Hodge 1979) structures (Table 1). In larger, and generally older, structures this may also involve subsequent burial, as in the case of Eagle Butte and Steen River (Robertson and Grieve 1975), Obolon (e.g., Gurov et al. 2009), or Chesapeake Bay (Poag et al. 1992), or even tectonism as at the Sudbury impact structure (Dietz 1964). The result of low levels of preservation is that a single terrestrial crater rarely provides a complete record of the processes involved with its genesis. The Whitecourt crater provides a rare exception in that it is well preserved, has an intact and easily observable ejecta blanket, and associated meteorites. As well, because researchers were the first to document the site, the distribution of these features has not been compromised from private collections. A summary of known terrestrial impact structures of similar dimensions and age to the Whitecourt crater is provided (Table 1).

The Whitecourt crater, located in central Alberta (Canada), represents a significant addition to the terrestrial impact record (Fig. 1). The <1,100 yr old crater, formed by the impact of a type IIIAB iron meteorite, is a simple bowl-shaped structure 36 m in diameter having a depth of approximately 6 m as measured parallel to the local hill slope (Herd et al. 2008). There are no other depressions associated with the crater to at least 2 square kilometers, aside from anthropogenic disturbances (Herd et al. 2008). The small size of the Whitecourt crater implies several possible formation scenarios, which vary in both impact velocity and impactor size. At the low-energy end of the impact spectrum, a penetration crater forms as a result of low impact velocities, typically less than a few hundred meters per second (French 1998). The impactor, in this scenario, would be expected to survive

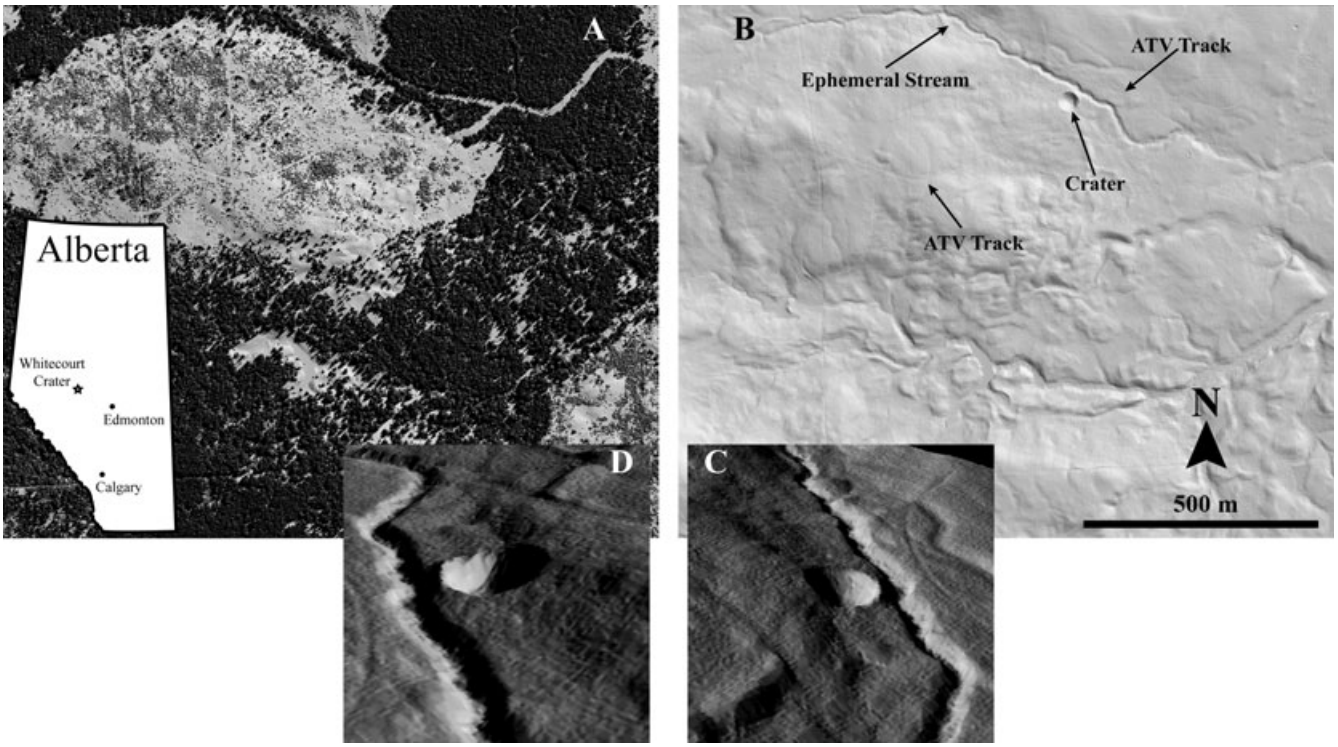

Fig. 1. A) Full-feature and B) bare-Earth LiDAR images of the Whitecourt crater, having the same scale, and surrounding area including oblique views looking C) northwest and D) southeast of the 36 m diameter crater from a LiDAR-derived digital elevation map. Access to the site was primarily along the all-terrain vehicle (ATV) track north of the crater.

Table 1. Known impact craters having similar dimensions and ages to the Whitecourt crater.[a] For sites containing multiple impact structures the diameter of the largest structure is reported.

Crater name	Location	Diameter (km)	Age (ka)[b]	Target material	Bolide type[c]
Campo del Cielo	Argentina	0.05	< 4	Loess[d]	Coarse octahedrite to granular hexahedrite
Carancas	Peru	0.0135	0.002	Unconsolidated sediment[e]	H4–5 chondrite[f]
Haviland	Kansas, USA	0.01	< 1	Unconsolidated sediment[g]	Pallasite
Ilumetsä	Estonia	0.08	> 2	Sand/siltstone[h]	–
Kaalijärv	Estonia	0.11[i]	2.4[i]	Loess and dolomite[i]	IAB[i]
Morasko	Poland	< 0.09	3.5–5[j]	Unconsolidated sediment[j]	IAB coarse octahedrite[k]
Sikhote Alin	Russia	0.02	0.059	Loose sediment[l]	Hexahedrite
Sobolev	Russia	0.05	< 1	Mixed[m]	Iron meteoritic material found
Wabar	Saudi Arabia	< 0.116	0.14	Loose sand[n]	IIIAB

[a]Obtained from the Earth Impact Database (2006) unless otherwise noted.
[b]Pre-1977 K-Ar, Ar-Ar, and Rb-Sr ages recalculated using the decay constants of Steiger and Jager (1977).
[c]From Koeberl (1998) unless otherwise noted.
[d]Cassidy et al. (1965).
[e]Brown et al. (2008).
[f]Brown et al. (2008).
[g]Hodge (1979).
[h]Raukas et al. (2001).
[i]Reinvald and Luha (1928), Kracher et al. (1980), Rasmussen et al. (2000), and references therein.
[j]Stankowski (2001) and Stankowski et al. (2007) and references therein.
[k]Dominik (1976).
[l]Lang and Kowalski (1973).
[m]Mixed implies sedimentary strata overlying crystalline rock.
[n]Shoemaker and Wynn (1997).

relatively intact and remain buried within the immediate vicinity of the crater. The diameter of the resulting penetration crater is limited to a maximum of several times the diameter of the impactor. At higher velocities, dependent upon the speed of sound in the target and impactor materials, explosively excavated craters result from high velocity or hypervelocity impact—generally at least 3 km s^{-1} for most metals (e.g., Fair 1987). The impactor, in this scenario, would not survive as a single coherent mass. The fate of the impactor, whether it fragments, melts, vaporizes, or some combination of the three, is controlled primarily by impact velocity. These scenarios will be addressed qualitatively.

In order to address the possible impact scenarios, we present field evidence collected between 2008 and 2009. These data allow constraints on parameters surrounding the Whitecourt impact event including the impact angle, impact velocity, and fate of the impactor.

REGIONAL GEOLOGY

The Whitecourt crater developed in sediments associated with the advance and retreat of the Laurentide Ice Sheet, which unconformably overlie fluvial sedimentary rocks of the Paleocene Paskapoo Formation. This provides a succession of Cretaceous to Tertiary sedimentary bedrock capped by Quaternary glacial deposits that dominate the regional geology near the crater. The Paskapoo Formation, a heterogeneous fluvial mudstone and sandstone complex, comprises the local surface bedrock (Tokarsky 1977; Grasby et al. 2008). The overlying glacial deposits are dominated by fine-grained till, part of the Prairie-Mackenzie (till) Province, of which over 80% is derived from local bedrock, and contains approximately equivalent parts of sand, silt and clay (Scott 1976).

Outcrops located within several kilometers of the Whitecourt crater provide insight into the association of the local bedrock and glacial till. These outcrops consist of a thin veneer of till sharply overlying clean unconsolidated massive-to-bedded fine sand. Till thickness varies significantly, at one site thickening by about 6 m over a horizontal distance of approximately 15 m. At each outcrop <3 m of massive unconsolidated sand is exposed. At two outcrops the base of the exposure reveals a sharp contact between the sand unit and a laterally discontinuous thin blocky mudstone or platy sandstone. The sediments underlying the glacial till are likely part of the Lacombe Member of the Paskapoo Formation, characterized by siltstones, mudstones, channel and splay sandstones (very fine to medium grained), with minor coal beds. At the surface, this unit is commonly unconsolidated or only weakly consolidated; it may reach thicknesses of up to 300 m (Demchuk and Hills 1991; Grasby et al. 2008).

The local surface soil is an orthic gray luvisol (Soil Classification Working Group 1998). The profile consists of decomposing forest litter (O horizon—<15 cm thick) overlying a dark, organic-rich, silty-very-fine sand (Ah horizon—<10 cm thick), sharply overlying a pale silty-very-fine sand (Ae horizon—<30 cm thick). Below the Ae horizon there is a gradational increase in fines observed in pore spaces and as grain coatings. At the Whitecourt crater this transition zone (Bt horizon) is often thin and poorly defined. The parent material, at the base of the profile, is a pale gray to dark brown glacial till containing rare clasts up to approximately 15 cm in diameter (C horizon). The till is composed primarily of equal parts clay, silt, and very fine sand. Granite and gneiss clasts represent the dominant lithic fragments within the till with less frequent cm-scale mudstone and sandstone clasts.

The Whitecourt crater is found on a narrow northeastward sloping terrace immediately south of an ephemeral stream (Fig. 1). The target sediments consist primarily of glacial till and, to a lesser extent, massive unconsolidated-to-weakly consolidated fine sand (of the Lacombe member of the Paskapoo Formation).

METHODS

Work at the site focused on surface and subsurface investigations in addition to the search for meteorites. Surface elevation data and horizontal positioning were obtained primarily through the LiDAR data obtained from Airborne Imaging, Inc. (Calgary, Alberta). The locations of soil pits, auger holes, and meteorites were recorded using handheld GPS units though, in most cases, these data were augmented by additional measurements. An Eijkelkamp hand auger, capable of reaching depths over 6 m, was used for subsurface sampling. The sampling chamber at the boring end of the auger is capable of providing a moderately undisturbed view of the sediments at approximately 10–15 cm intervals (Fig. 2). Subsurface information was collected primarily from soil pits for depths typically < 0.5 m and auger holes for deeper observations. We documented over 50 sample sites in addition to meteorite locations. Two cross sections generated from these sample sites delineate both the ejecta blanket, identified as the material overlying a local buried soil, or paleosol (Fig. 2), and the crater fill distribution.

Sediments obtained from varying depths and locations were analyzed either in bulk or as sieved samples. In particular, we were interested in finding evidence of impact-generated melt or shock effects. Focus, therefore, was placed on samples collected from

Fig. 2. An image of the contact between the ejecta and the top of the paleosol, organics (charcoal), and underlying Ah horizon, used to delineate the ejecta blanket as revealed in the sample chamber of the auger. In this image, the overlying ejecta represents ejected Ae horizon material. Way up is to the left.

medial and distal ejecta in addition to sediments collected near the base of the transient crater boundary, where the greatest concentration of the most strongly shocked materials are expected (e.g., French 1998). Magnetic grains collected from these samples were analyzed using a stereo microscope and, in select cases, a JEOL 6301F field emission scanning electron microscope (SEM). To search for nonmagnetic melt and potentially shocked grains, sediment samples were sieved either using a no. 200 (75 μm) or a no. 230 (63 μm) sieve and the residue analyzed initially using a stereo microscope. Quartz grains collected from the residue were subsequently viewed through an optical microscope using immersion oils (n = 1.572 and 1.550) to search for planar fractures (PFs) or planar deformation features (PDFs) commonly associated with impacts (see Grieve et al. 1996 for a review). The filtrate of several proximal and distal ejecta samples were also analyzed quantitatively to search for evidence of atmospheric sorting.

Members of the research team, a number of Whitecourt area residents, and several other volunteers were involved in the documented search for meteorites. The search was conducted primarily with metal detectors, though a magnetometer was also used. Where possible, meteorites were photographed in situ with markers indicating magnetic north. This was done for several samples having masses >300 g, collected during the latter part of the field campaign. Magnets were used to collect samples too small to easily identify or collect by hand, commonly for meteorites less than approximately 0.5 cm in longest dimension.

To investigate the possibility of a large buried mass being present at the site we conducted several magnetic and gradiometric surveys using GEM Systems' GSM 19-TW and the more sensitive 19-GW magnetometers. It was expected that such surveys would reveal magnetic anomalies that may be associated with the large buried mass required to form a penetration crater this size (possibly >10 m in diameter). Due to the failure of the GPS sensor on the 19-GW, this instrument was used only to locate anomalies within the structure. A 100 m by 100 m grid centered on the crater was set up and walked using the 19-TW. The rover recorded measurements at 0.5 s intervals whereas the base station recorded measurements at 3.0 s intervals.

Chemical analyses of the meteorites at the crater are restricted primarily to the weathering products of several sub-centimeter fragments. These meteorite fragments were collected from the top of the contact between the diamict and massive unconsolidated fine sands approximately 2.9 m beneath the base of the crater. Two fragments were mounted in epoxy, sectioned, and polished. We analyzed sections using a Cameca SX100 electron microprobe to generate X-ray elemental maps using wavelength dispersive spectrometry (WDS). Material from the weathered rind of a third meteorite collected from this depth was crushed using a mortar and pestle and then magnetically separated using a technique similar to that of Chen et al. (2005). The resulting magnetic material was analyzed using a Rigaku Geigerflex Power Diffractometer (XRD). The remainder of the collected meteorites were cleaned using deionized water, acetone, and soft brushes.

RESULTS

The Impact Crater

The fact that the Whitecourt crater has remained unidentified for so long attests to the obscuring nature of the local topography, vegetation, and its relatively small size (Fig. 1). The site is located within 40 m of two well-used all-terrain vehicle (ATV) tracks, though only partially visible from the north track during the winter months (Fig. 3). Local topography also introduces some variation in the actual crater dimensions, notably in crater depth. The rim elevation of the Whitecourt crater varies by approximately 5 m resulting in an apparent depth range from approximately 5 m, as measured at the east rim, to approximately 10 m, as measured from the south rim. These measurements supplement the depth as measured parallel to the local slope as reported by Herd et al. (2008).

The overall structure of the Whitecourt crater is similar to most simple bowl-shaped terrestrial craters with only a few exceptions. An overturned flap located near the crater rim, commonly associated with simple structures, has not been observed at any of the sample sites located along the crater rim. It is unclear why this is the case; the thickness of, and contrast between the

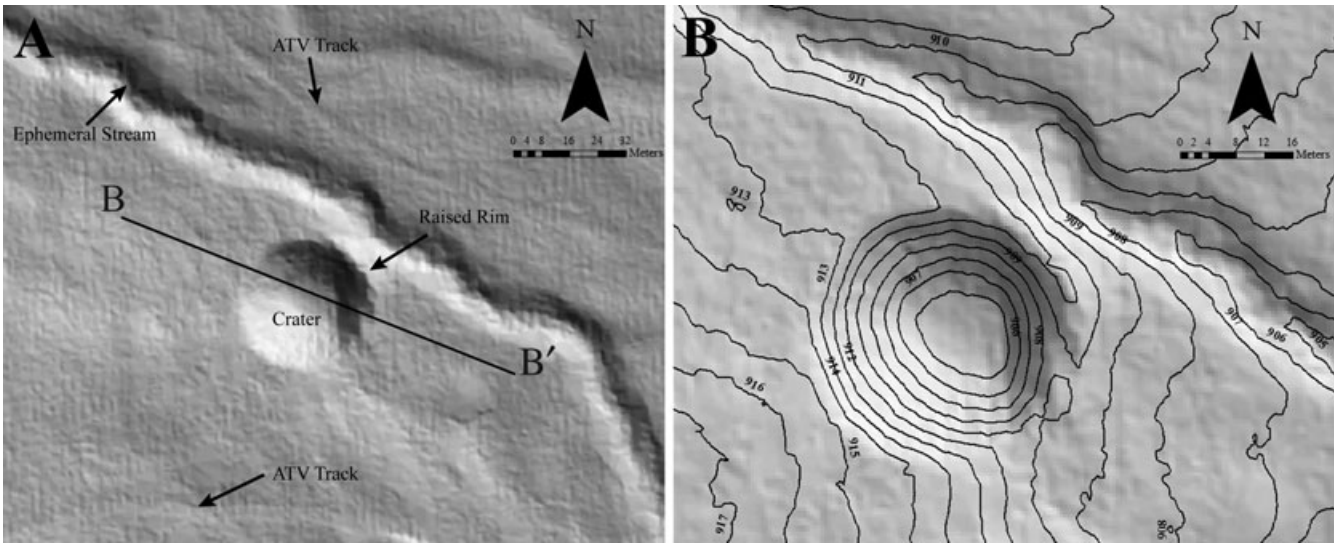

Fig. 3. A) Bare-Earth LiDAR image of the crater and nearby surroundings. B) Surface contours at 1 m intervals.

unconsolidated very fine sand (Ae horizon) and the relatively cohesive glacial till (C horizon) may have prevented the overturned flap from developing. It is also worth noting that the raised rim, which typically circumnavigates simple craters, only extends between the bearings approximately 020° and approximately 110°. The opposing side of the crater shows little evidence of uplift. Given the gentle topography of the target surface, it is unlikely that the hill slope played a significant role in determining the crater rim morphology. The asymmetry of the raised rim observed here may be analogous to a depressed up-range rim and is discussed later. Surface contours within the crater are relatively circular and evenly spaced indicating that there has been no preferential crater wall steepening (Fig. 3). The high elevation of the south rim is likely responsible for the distortion of the contours along that wall as tree trunks along the south wall show some evidence of creep.

Glacial till and, to a lesser extent, unconsolidated to weakly consolidated fine sand dominate the target sediments. Within the immediate vicinity of the crater, we were unable to determine the actual thickness of the till. At a site 18.5 m east of the crater rim the till reaches a thickness of at least 5.8 m, though this may not represent the thickness of the till at the point of impact (Fig. 4). The local till has consistent silty clay texture and only appears to vary in color. The well-sorted, unconsolidated massive fine sand present beneath the crater at depths below approximately 2.9 m to approximately 3.45 m is similar to the fine sand observed at outcrops near the crater, in the crater fill, and as small centimeter-scale sand lenses in the ejecta east and northeast of the crater. It extends to a depth of at least 5.41 m below the base of the crater floor; the local water table is still below this depth. Subangular to angular quartz grains represent the bulk of the fine sand. No clear depositional structures were observed within this sand unit, though it is possible that structures present at these depths have been obscured by the impact and/or the process of sampling. Figure 4 provides a general overview of the crater and target sediments.

The crater fill is largely a diamict, more heterogeneous than the local till observed in the area. Centimeter- to decimeter-scale sand lenses are common in the crater fill, but are not observed in the local till. In addition, there is a coarse sand component present in much of the observed crater fill, likely derived from the underlying fine sand. Fragments of sandstone, similar to those observed at outcrops in the area, are also present within the crater fill. These fragments appear to be concentrated along the east crater wall and are up to 20 cm in longest dimension and typically approximately 1.5 cm thick. Contacts between the crater fill and the local till are found at depths of 1.35 m and 2.55 m along the east and west crater walls, respectively (Fig. 4). The underlying diamict at each contact is consistent with till located outside the area affected by the impact. We interpret the transition between the crater fill diamict and the massive unconsolidated sand at approximately 2.9 m and approximately 3.45 m beneath the crater floor to mark the depth to the transient crater boundary at the center and northeast corner of the crater floor, consistent with the interpretation of Herd et al. (2008) (Fig. 4). The depth of the transient crater is, therefore, between approximately 9 m and approximately 9.5 m as measured from the crater rim

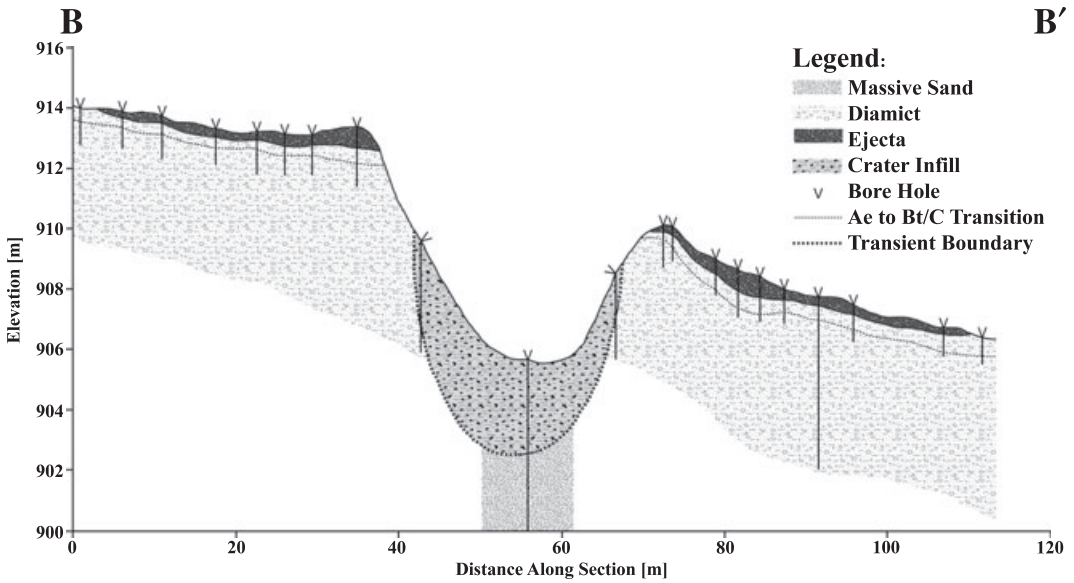

Fig. 4. Summary cross section through the crater along 110° (Fig. 3). For simplicity the various soil horizons are not shown. While the ejecta blanket is capped by an O and thin Ah horizon, a well-defined Ae horizon is not observed. The transient crater boundary is constrained by five auger holes (the fourth and fifth are not included in this section). The base of the transient crater boundary is likely more irregular than displayed, due to the changes in sediment type. The center of the transient crater appears slightly offset toward the northeast. The depth to the transient crater boundary is approximately 2.9 m at the center of the crater floor (Herd et al. 2008) and approximately 3.45 m along the northeast crater floor—the surface is at the same elevation. The vertical exaggeration is 4.2.

parallel to the local hill slope; it is roughly between 8.5 and 9 m deep as measured from the pre-existing surface along the same orientation.

Conclusive evidence of shock within the crater fill is limited. Parallel planar microstructures (PM) in quartz grains are common within the fine sand beneath the transient crater boundary (Fig. 5). However, almost all grains exhibiting parallel PM contain only one to three sets resolvable using optical microscopy. The apparent spacing of the measured PMs is approximately 5 μm. We have found no silicate melt and only rare samples of impactor melt within the crater fill, and below the transient crater boundary (Fig. 5).

The Ejecta Blanket

Mapping the distribution of the ejecta blanket and determining its approximate volume was one of the primary objectives of the investigation at the Whitecourt crater. LiDAR imaging does not resolve the ejecta distribution. Additionally the LiDAR data reveal no surface features (grooves, ridges, ramparts, or other forms providing evidence of radial flow) typically associated with nonterrestrial ejecta blankets. The ejecta distribution was determined by mapping the depth to the surface of the underlying paleosol (Figs. 2 and 6), using auger holes and soil pits. This paleosol is continuous in the area adjacent to the crater and provides a reference point for the thickness of the ejecta blanket. Figure 6 shows the location of soil pits and auger holes used to map the ejecta blanket. Using the depths and locations of the paleosol observed at the site, the original surface sloped approximately 9° to the east-northeast.

There is some variation in the organic content at the top of the paleosol, a fragile dark organic-rich layer (Ah), 3 to 15 cm thick that is commonly capped with a thin layer of charcoal at the site. The preservation of the paleosol implies that the ejected sediments were deposited at velocities low enough to prevent incorporation of the underlying surface material. At locations where the paleosol lacked significant organic material, the depth was delineated by the contact between the base of the ejecta and the top of the underlying Ah horizon. Charcoal from the paleosol surface provides a maximum age for the crater of approximately 1,100 cal yr BP—based on radiocarbon ages of 1,130 ± 25 and 1,080 ± 25 ^{14}C yr BP (Herd et al. 2008).

The ejecta blanket distribution was determined using a series of auger holes along two lines transecting the crater. Several additional auger holes and soil pits confirm that the ejecta blanket surrounds the crater. The thickness of the ejecta was measured along these transects and at various other sites (Fig. 6). These thicknesses were also used to estimate ejecta blanket

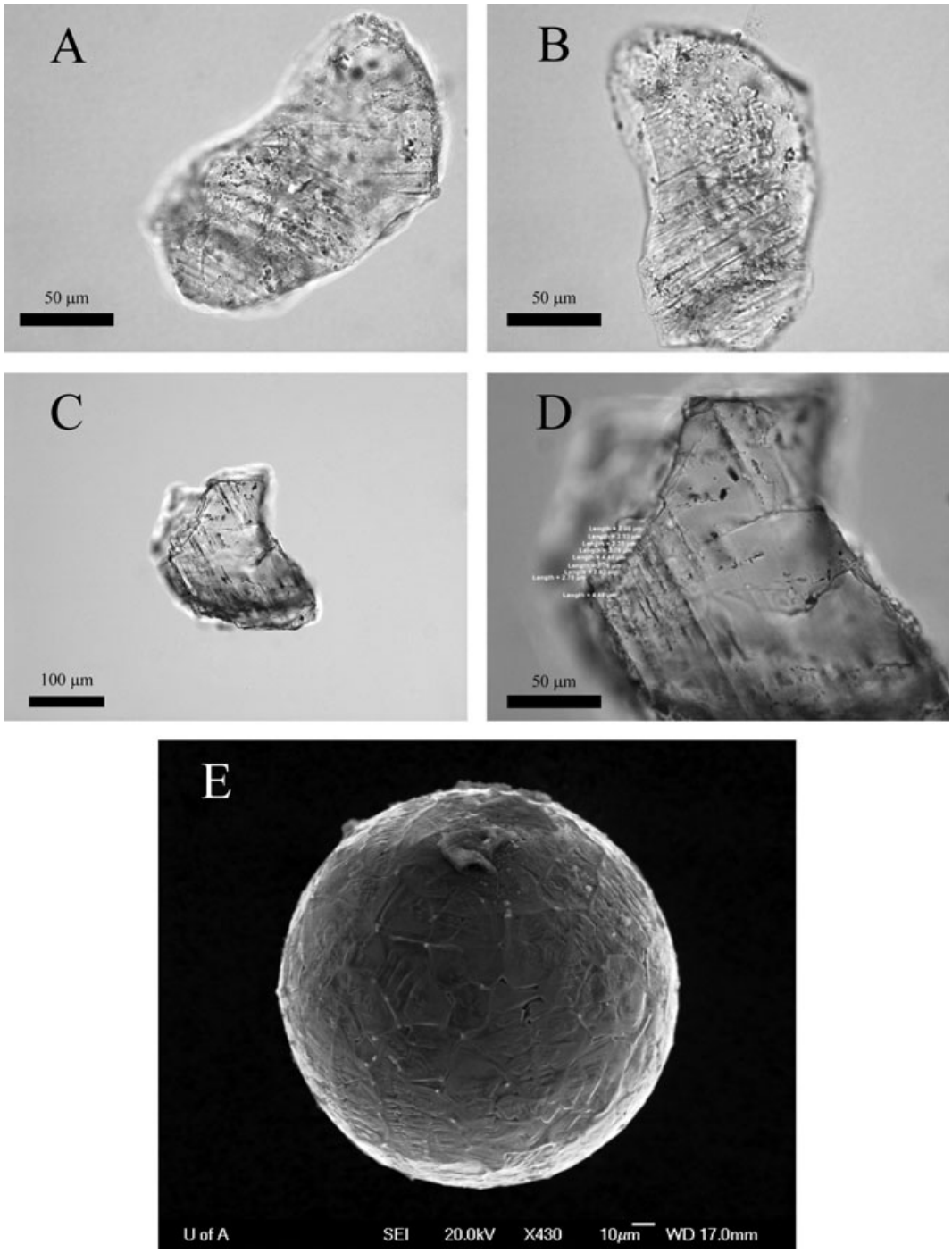

Fig. 5. A–D are two quartz grains exhibiting PMs. A and B are the same sample with a slightly different rotation and focal plane to show at least three sets of PMs. C) and D) are another grain displaying only a single set. Spacing measurement locations are visible on (D). The average apparent PM spacing is 4.85 μm for (A) and (B), and 3.26 μm for (C) and (D). The grains are mounted in immersion oil (n = 1.572) and photographed in plane-polarized light. Similar grains have been recovered at depths up to 4.62 m beneath the crater floor. E is an SEM image of a 180 μm diameter Fe-Ni oxide spherule collected at the Whitecourt crater. Recovery depth of (E) was 3.27 m beneath the northeast crater floor (Norm wt%: Fe = 68.17, Ni = 8.20, Al = 0.41, O = 22.71).

thickness in areas not sampled, allowing the volume of the ejecta blanket to be estimated. The resultant distribution indicates that the ejecta is concentrated to the east-northeast of the crater with limited bilateral symmetry. There does not appear to be a significant zone of avoidance, or forbidden zone, characterized

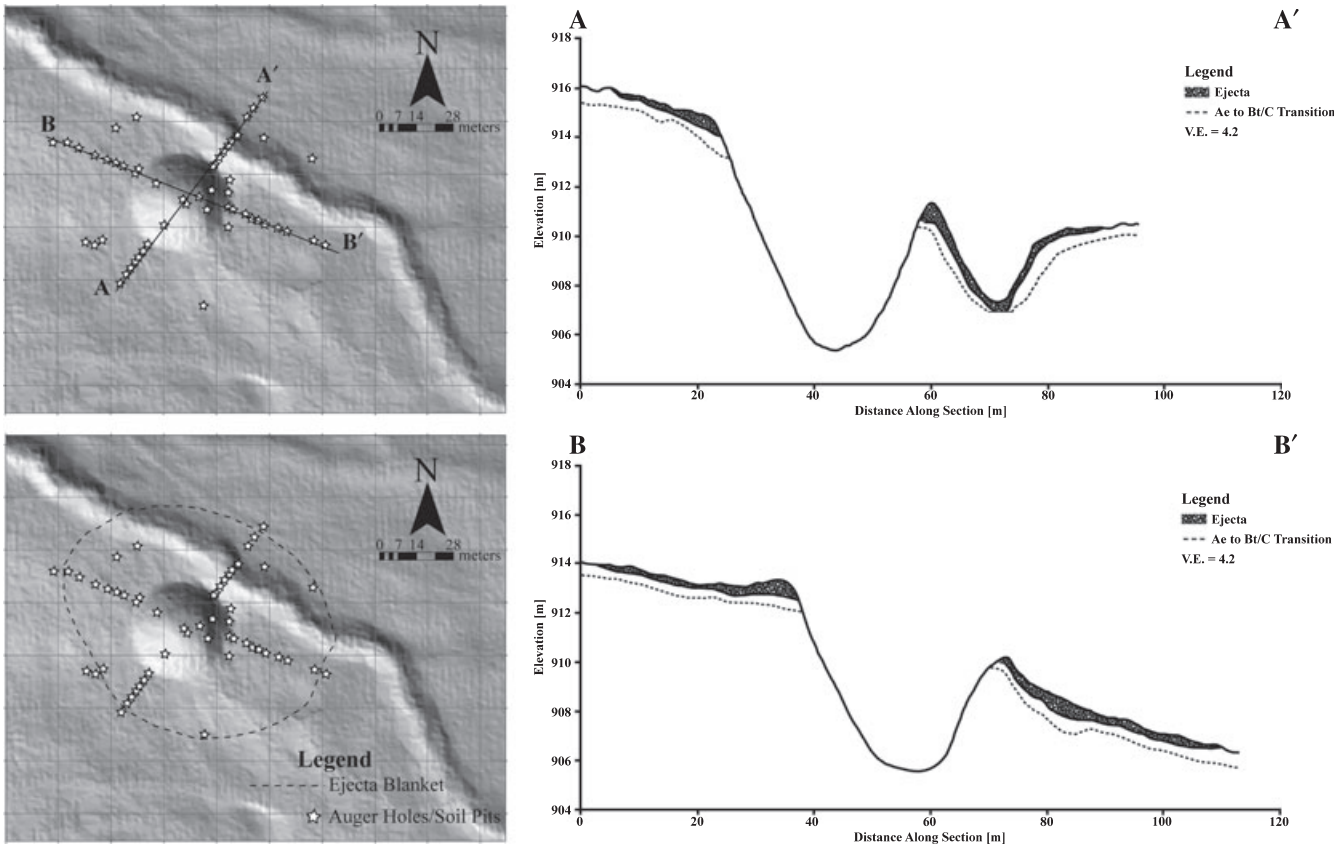

Fig. 6. Cross sections of the ejecta blanket along 038° and 110° with a reference figure showing the location of the sections. Approximate distribution of the ejecta blanket and the main soil pit and auger hole site locations are also provided.

by a lack of ejecta (e.g., Schultz 1992c). Based on analysis using ArcGIS software, the ejecta covers an area of approximately 6000 m^2, and has a volume of approximately 1250 m^3 based on the distribution shown (Fig. 6), representing roughly 40% of the approximately 2900 m^3 crater volume (Herd et al. 2008).

The ejecta blanket is composed of three units. The two main units are diamict (derived from the target Bt/C horizon) and very fine sand (derived from the Ae/Ah horizon). The third unit is fine sand, which is similar in appearance to the fine sand observed at depths >2.9 m (C horizon) beneath the crater floor and at several outcrops near the crater. No large (decimeter-scale) fragments of sandstone have been observed within the ejecta blanket. The most proximal ejecta consists only of the two main ejecta units, diamict and very fine sand (Fig. 7). The very fine sand and diamict are strongly disturbed, and vary in unit size and distribution. The sharp contacts between these units suggest that subsequent modification due to soil forming processes is limited. There does not appear to have been significant mixing between the two units during excavation and deposition within the nearest 5 m of the crater rim, consistent with the lower energies involved in proximal ejecta emplacement. The thickness of the most proximal ejecta varies between approximately 25 cm and approximately 80 cm.

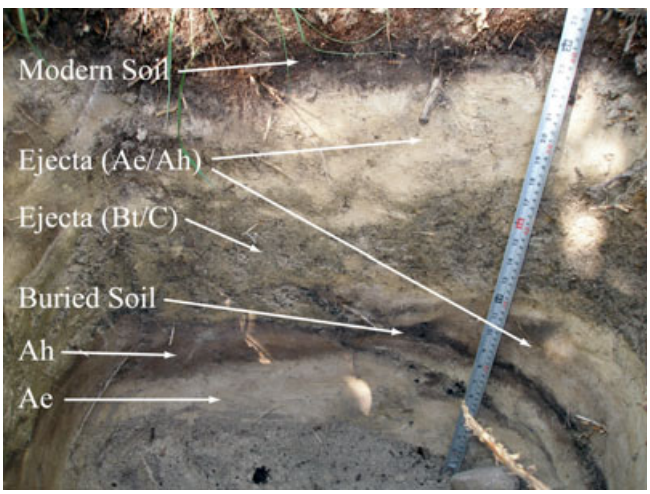

Fig. 7. Proximal ejecta located at the first sample site southwest of the crater rim along the A–A′ (Fig. 6). The horizons indicated are disturbed, and represent sediment from which the ejecta was derived.

Fig. 8. Images of the ejecta from proximal to distal (left to right). The center image includes an in situ meteorite (circled) toward the top right at the base of the modern soil.

At roughly one-third extent from the crater rim along each transect only a single unit is observed. Diamict comprises the dominant unit beyond this point, though the northern portion of the A–A′ transect has A horizon material at its terminus. The other three terminal points of each transect, and pits in more distal locations, all have diamict as the ejected material. No deposition structures were observed within the ejecta (Fig. 8).

Qualitative assessment of proximal and distal ejecta samples provides little evidence of sorting. Several samples filtered using a no. 200 (75 μm) sieve show only minor differences in silt and clay content per volume sampled. In general, there appears to be a slightly higher proportion of silts and clays in the most distal material, though it remains a poorly sorted diamict. This difference could arguably relate to heterogeneity in the diamict itself and not necessarily to atmospheric sorting.

No clear shock effects were observed in the ejecta. We found no melt products within the proximal, medial, or distal ejecta. Magnetic grains are common within the till, including rare millimeter-scale meteorite fragments. However, magnetic grains recovered from the ejecta appear to predate the impact and are present in till not affected by the event. Quartz grains containing single sets of parallel PM are present, though rare, in medial and distal ejecta samples. Their rarity is likely due, in part, to the difficulty of working with the smaller quartz grain sizes present in the ejected sediments. The orientations of these PM have not been determined. It is worth noting parallel microstructures, while present, are extremely rare in quartz grains collected from the fine sand collected from other Paskapoo Formation outcrops; these samples are not as planar as those observed in samples from the crater, and are likely the result of much older tectonism.

The Meteorites

The recovery of meteorites led to the discovery of the crater, which was known initially as an unusual depression to a number of local residents for over a decade. Little was thought of the depression until two individuals brought it to the attention of the authors. James R. ''Sonny'' Stevens and Rod Stevens decided to search for meteorites at the site (Herd et al. 2008). Since their initial discovery, over 2500 meteorites have been collected with a cumulative mass approaching 70 kg.

The meteorites, with few exceptions, have similar jagged and angular morphologies (Figs. 9A and 9B). Cut samples reveal the Widmanstätten pattern characteristic of type IIIAB irons and include areas where the pattern was disrupted due to recrystallization (Herd et al. 2008), suggesting that their internal structure controls, in large part, their external morphology. In addition, the present suite of meteorites contains only a single 6.51 kg sample displaying evidence of well-defined atmospheric modification, including regmaglypts, which are distributed along its entire surface, and a partially exposed fusion crust (Fig. 9C). This sample likely represents a fragment that

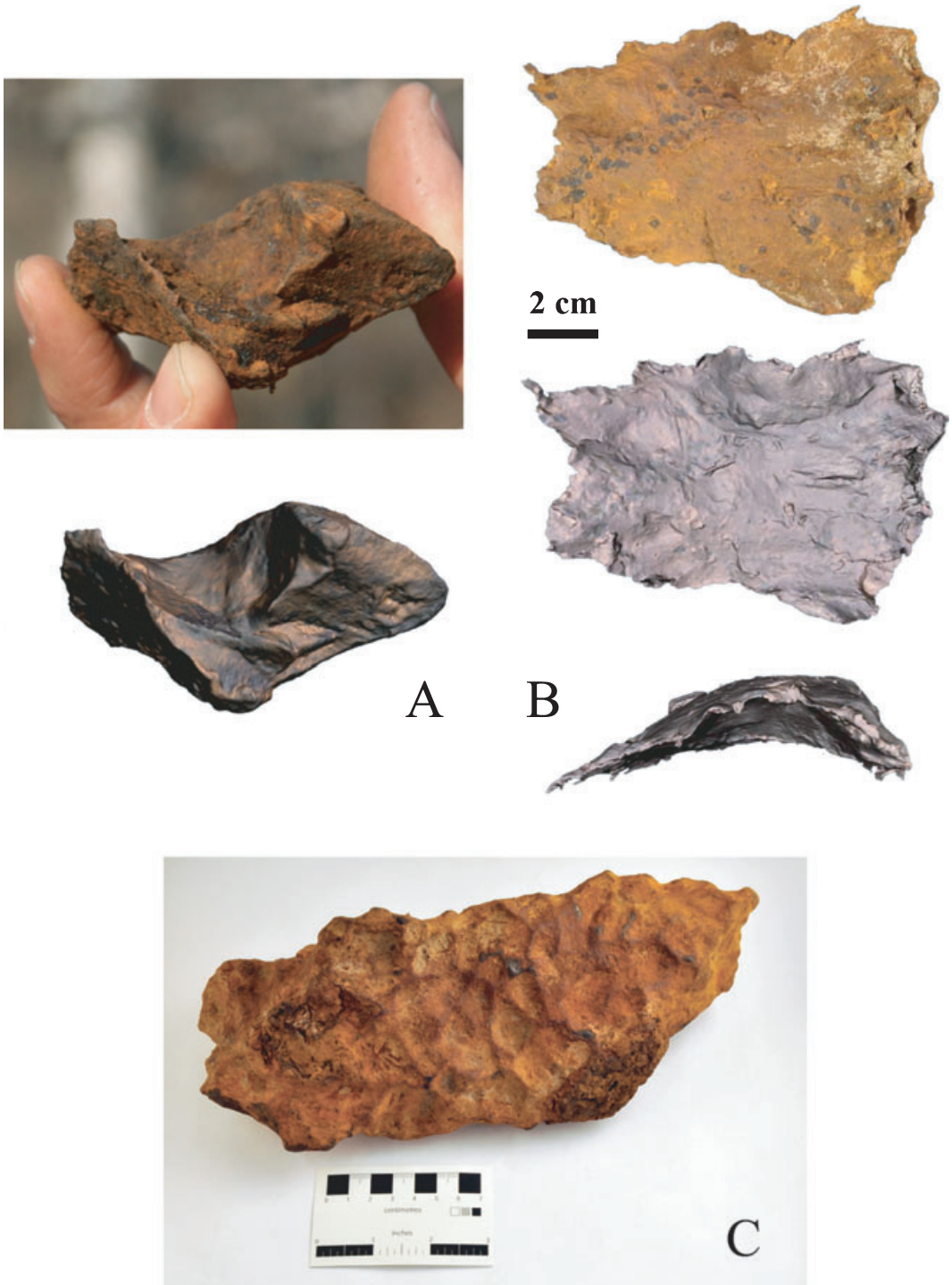

Fig. 9. Images of two meteorites and their associated 3D scans. The masses of the samples are (A) 254 g and (B) 855 g. The photographs were provided by (A) Marie-Claude Williamson, Canadian Space Agency, and (B) Tiffany Borgel, University of Alberta. The 3D scans were generated by (A) R. Kofman and (B) Chris Want, University of Alberta, using a NextEngine desktop 3D laser scanner. The 6.51 kg meteorite (C) was found approximately 261 m east-northeast of the crater (Fig. 10). This sample's surface is characterized by regmaglypts and an exposed fusion crust. Photograph by R. Kofman.

spalled off the main mass shortly after entering Earth's atmosphere. The remaining samples lack a preserved fusion crust, atmospheric sculpting effects, and regmaglypts. However, several of the Whitecourt meteorites arguably represent fragments initially situated at the surface of a larger body, which

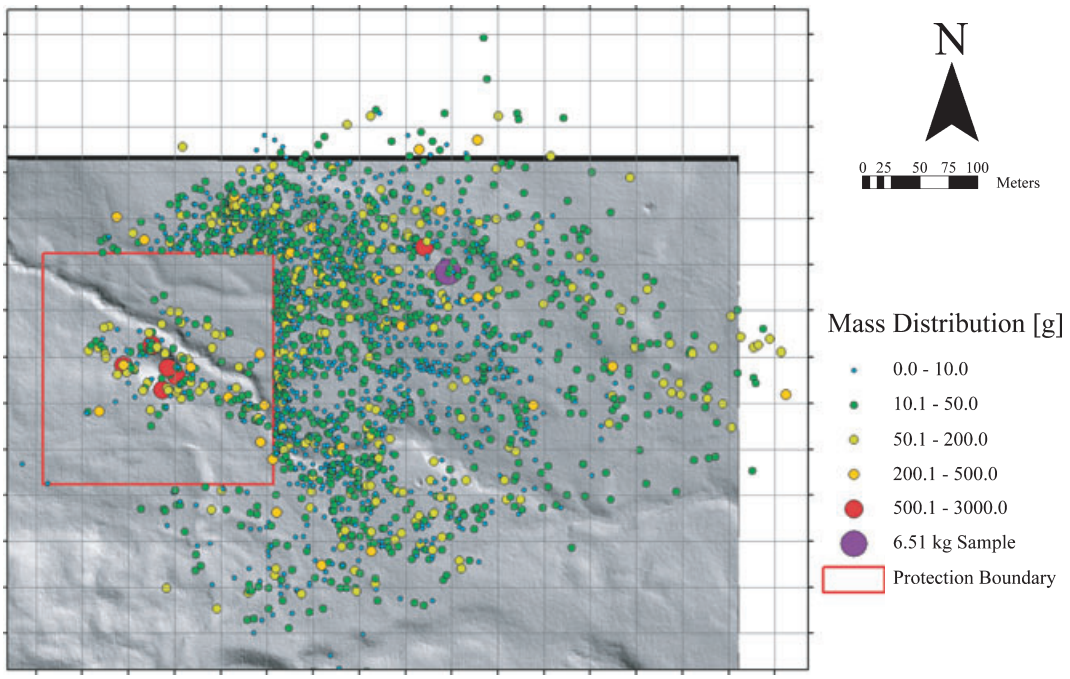

Fig. 10. The mass distribution of meteorites at the time of writing. The distribution extends beyond the range of the LiDAR data. Many sites contain multiple samples. The grid spacing is 50 m.

subsequently spalled off exposing a fresh unmodified surface with jagged edges.

Figure 10 illustrates the known meteorite distribution. As of July 2010, most of the samples represent material collected by a volunteer search team outside the 200 m by 200 m area protected under the Alberta Provincial Historic Resources Designation Act (Herd et al. 2008); meteorite searching within the protected area is limited in order to preserve the crater and ejecta blanket. The distribution fans out along 075° to 085°, with most samples between 000° and 130°, and the crater located nearest the west-southwest boundary of the distribution. The largest samples, those >200 g, range from within the crater to over 500 m beyond the crater rim. Fragments of meteoritic iron, having a mass <1 g, have been collected at both distal and proximal sites. At present, the most distal recovered sample is located over 520 m east of the crater rim. While the search for meteorites outside the protected area has focused on the northeast and southeast quadrants, searches were also conducted in the northwest and southwest quadrants with little success. The apparent concentration of smaller samples outside the protected area reflects, in part, the increased sensitivity of the detectors used by the volunteer team.

The bulk of the meteorites have been collected at depths <25 cm, typically near the base of the modern soil. With few exceptions, meteorites found in association with the ejecta blanket lie at, or near, the upper contact with the modern soil (Fig. 8 center); this may be due to the limited penetration depth of the metal detectors used to search near the crater. Where observed in situ, discoidal and dished meteorites typically lie flat with no evidence of preferred orientation (i.e., neither concave-up nor concave-down orientations appear favored). Meteorites found at greater depths within the ejecta are typically at depths <35 cm. These samples also show no preferred orientation. Meteorites collected beyond the range of the ejecta are typically located near the base of the modern soil; the deepest (Fig. 9C) was recovered from a depth of approximately 40 cm.

Meteorites were also collected from various depths within the crater fill and immediately above the transient crater boundary. As these meteorites were collected in the sample chamber of the auger head they are necessarily small, all <5 g. In addition to the small meteorites collected near the transient crater boundary, dozens of micro- to millimeter-scale meteoritic metal fragments were collected from sediment recovered above and below the transient crater boundary. This "meteorite dust" (Krinov 1966) is typically restricted to within 20 cm of the transient crater boundary with the bulk concentrated above, though some has been recovered from discrete lenses at shallower depths within the crater fill. Two larger, unrecovered meteorites were found, one at the transient crater boundary and another within the crater fill at a depth of approximately 1.4 m along the south crater wall. These

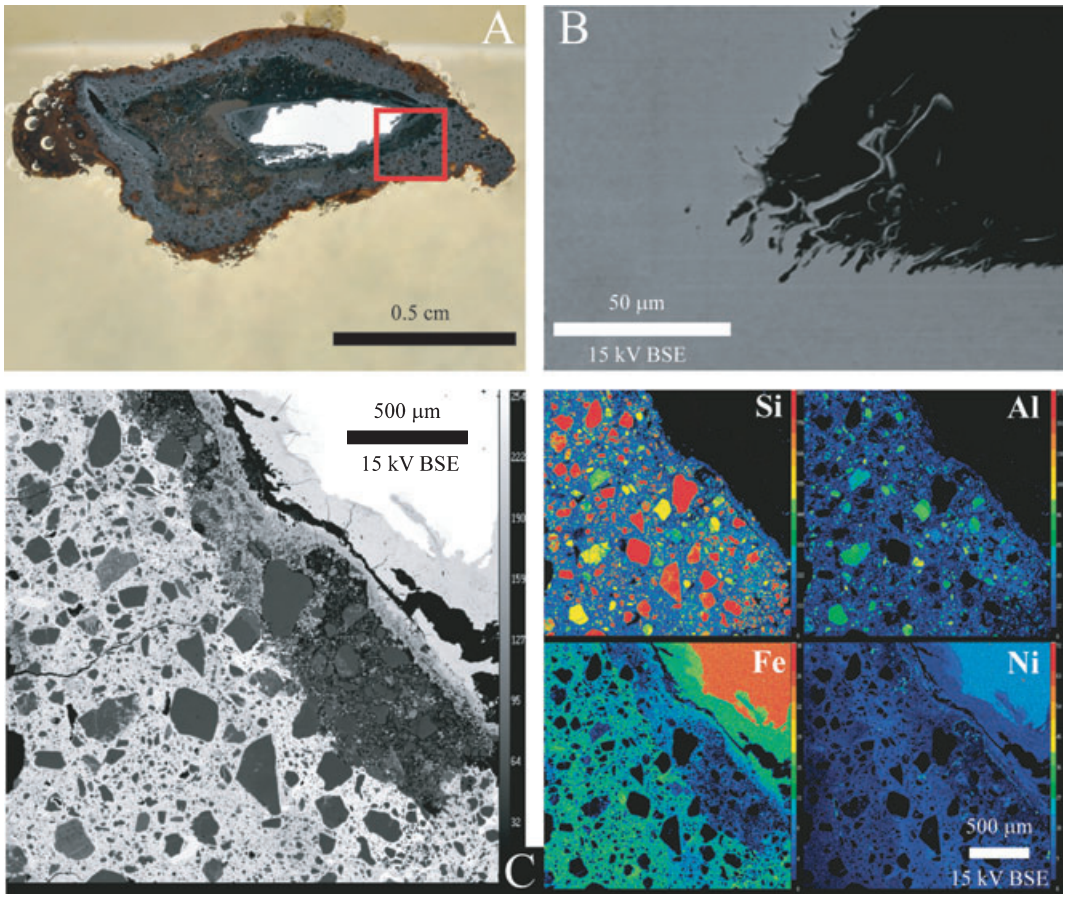

Fig. 11. A) A shale ball collected from the base of the transient crater. B) A backscattered electron image of well-preserved filament-like surface texture on the metal core of one of the shale balls. The gray material in the image is meteoritic iron. C) BSE image and elemental maps revealing the qualitative distribution of Si, Al, Fe, and Ni for a portion of the shale ball delineated by the red square in (A).

unrecovered meteorites have probable masses of several hundred grams.

A number of the small meteorites recovered at the transient crater boundary are analogous to the "shale balls" observed at Meteor Crater (Barringer 1909; Artemieva and Pierazzo 2009). The shale balls are, in this case, clasts of Fe-stained, Fe-oxide cemented target materials with meteoritic iron cores (Fig. 11A). While it appears that there has been some weathering, particularly as evidenced by the diffusion of Ni from the fragment into the surrounding materials, it seems that the weathering process was relatively quick and/or short-lived, possibly halting once the weathered rind had formed. The brief weathering duration would explain the preservation of such fine textures and structures still preserved at the surface of the fragment (Fig. 11B). These shale balls show more terrestrial alteration than the other meteorites. XRD analysis of these samples indicates that the dominant alteration products are goethite and magnetite/maghemite. The dense rind encapsulating the sample delineates the local limits of Fe and Ni diffusion (Fig. 11C). In contrast, the near surface meteorites, while showing signs of weathering, rarely have any local sediments cemented or otherwise fused to their surfaces. The resulting weathered rind on most near surface meteorites is typically several tens of micrometers to a millimeter thick, which in places has produced flaky textures. In rare cases, weathering has exposed the Widmanstätten grid.

Data obtained from one of the magnetometer surveys reveal a number of positive and negative anomalies (red and green respectively in Fig. 12). Subsequent investigations of these anomalies have yielded several of the largest meteorites collected to date. At present, all of the anomalies found in the surveys appear related to near surface meteorites or magnets. With the meteorites removed, future surveys and forward modeling of the resulting data should provide a better view of the crater and immediate surroundings.

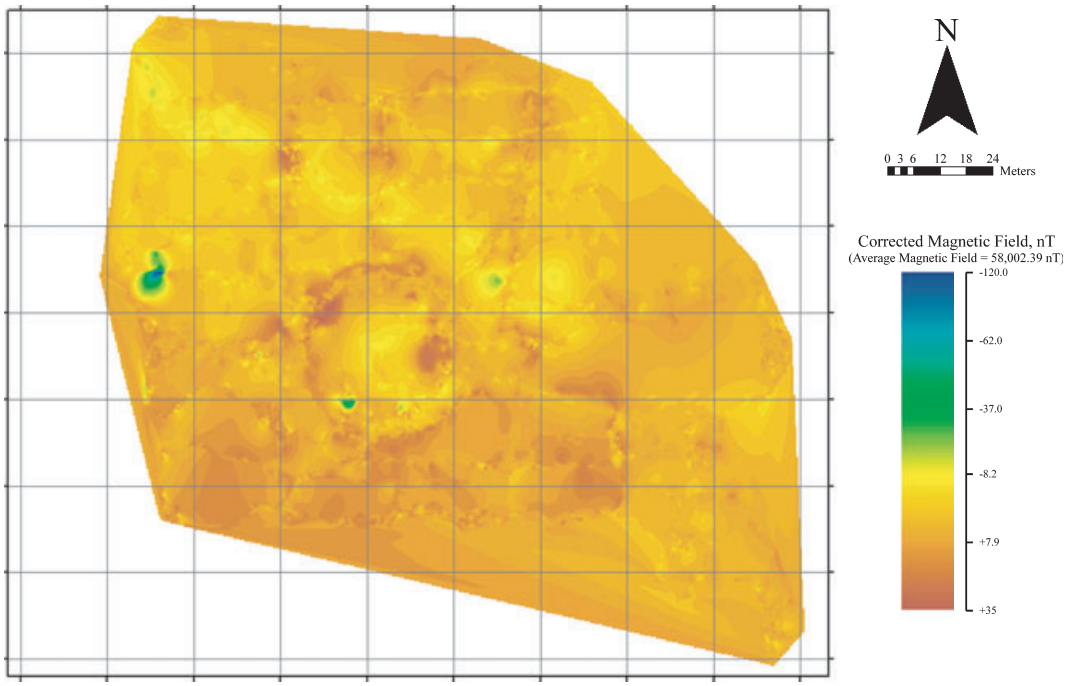

Fig. 12. Combined results of two magnetic surveys performed using the GEM Systems GSM 19-TW. This represents the diurnally corrected data. Dense vegetation along the southern half of the grid made surveying slightly more difficult. A large magnet was found at the large positive anomaly on the NW crater rim (one of three found to date, likely left behind by meteorite hunters). With the exception of the magnet, large meteorites, about several hundred grams each, were found at all the major anomalies. Several other meteorites of similar scale were recovered from additional localized anomalies evident only in the raw data.

DISCUSSION AND CONCLUSIONS

In summary, the Whitecourt crater is a circular bowl-shaped simple structure 36 m in diameter having a depth range of 5–10 m. The crater floor is bowl-shaped, showing no evidence of having hosted standing water. The structure and underlying sediments, to a depth of at least 5.4 m, are located above the local water table. The crater walls do not show significant steepening along any orientation, though creep is apparent along the southern wall. An impact-generated raised rim exists only along the northeast portion of the crater rim (Fig. 3). The well-preserved ejecta blanket lacks a forbidden zone and is concentrated east-northeast of the crater. Shock effects observed within the ejecta blanket, crater fill, and underlying sediments are limited to PM-bearing quartz grains, meteorite dust, and rare Fe-Ni oxide spherules, indicative of relatively low shock pressures and disruption and partial melting of the impactor. The associated meteorites, with one notable exception (Fig. 9C), are typically jagged and show little evidence of high-velocity atmospheric transit alteration effects. The meteorites are concentrated near the base of the modern soil surrounding the crater; however, several have been collected from greater depths within the ejecta and crater fill. Meteorite dust and several centimeter-scale meteorite fragments were also collected from the transient crater boundary.

At the Whitecourt crater a combination of crater morphology, ejecta blanket, and meteorite distributions constrain the flight path of the impactor. Regarding crater morphology, these features include the location and extent of the raised rim, the crater walls, and overall shape. The circularity of the structure and lack of crater wall steepening along any specific bearing suggest an impact angle greater than approximately 30° (Gault et al. 1965; Gault and Wedekind 1978). The raised rim, located on the northeast portion of the crater, is directly opposite a region showing no evidence of structural lift along the southwest (Fig. 6, particularly along A–A′). It is unlikely that postimpact modification has masked any significant structural uplift along the entire southwest half of the crater. Consequently, this may be analogous to the depressed up-range rim observed on much larger lunar and Venusian craters, which occur at impact angles between 40° and 45° (Herrick and Forsberg-Taylor 2003). The depressed and raised rim should form along the impactor's trajectory, which suggests that the incoming projectile was traveling along approximately 065° (Fig. 13).

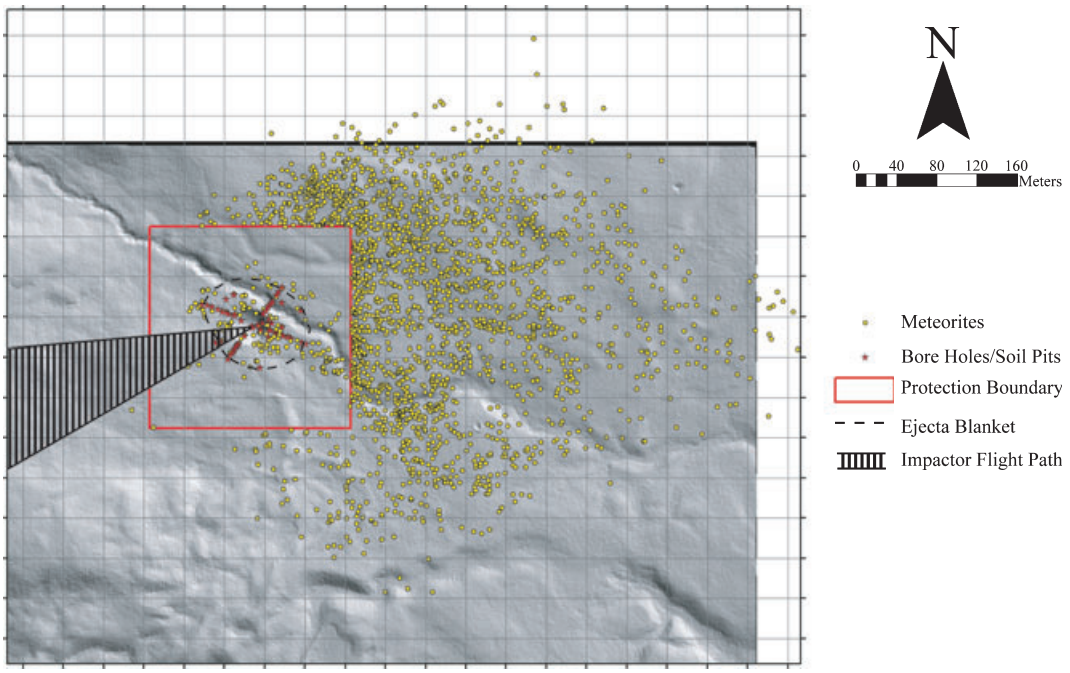

Fig. 13. A summary diagram, which illustrates the meteorite distribution, local sample sites and auger holes, ejecta blanket, and the proposed flight path of the impactor. Grid spacing is 50 m.

The distribution of the ejecta blanket provides another means of determining impactor trajectory. There is a clear concentration of ejecta toward the east-northeast with limited bilateral symmetry along that bearing (Figs. 6 and 13). On an airless body, the ejecta distribution remains axially symmetric to an impact angle as low as approximately 45° with the concentration shifting down-range as the angle decreases, though the presence of an atmosphere increases the angle at which this occurs (Gault and Wedekind 1978; Melosh 1989; Schultz 1992c). We have not observed a well-developed forbidden zone in the ejecta surrounding the Whitecourt crater. It has been experimentally determined that a forbidden zone develops uprange at impact angles typically <45° in a vacuum (Gault and Wedekind 1978; Melosh 1989; Schultz 1992c). This zone of avoidance develops at lower angles in the presence of an atmosphere (Schultz 1992c; Herrick and Forsberg-Taylor 2003). For Venusian craters (again, much larger than the Whitecourt crater), the ejecta blanket is concentrated downrange at angles <55°, slightly higher than would be expected on Earth (Herrick and Forsberg-Taylor 2003). Combining this with the crater morphology suggests that the Whitecourt impactor struck the surface at an angle likely between 40° and 55° while traveling toward approximately 060° to approximately 070°.

At terrestrial craters where meteorites are present, it is often possible to use their distribution to place constraints on the impactor's trajectory (e.g., Passey and Melosh 1980). In most cases, an incoming impactor will experience at least one major fragmentation event while traveling through the atmosphere resulting in its partial to complete disruption. The fragmentation process results in a large number of small fragments, which slow down and disperse, and a small number of large fragments, which maintain higher velocities and continue along a slightly modified trajectory. In an ideal situation for a significantly oblique trajectory, this will result in an elliptical strewn field in which the meteorites would be relatively well sorted having the largest fragments (and associated craters under favorable circumstances) concentrated down-range and the smallest fragments concentrated up-range. The long axis of the resultant ellipse would represent the direction of flight of the original impactor. In contrast, the distribution of the Whitecourt meteorites, being neither elliptical nor well sorted, does not appear to represent an ideal strewn field, though the distribution does appear to be controlled by the trajectory of the impactor. The direction of flight as constrained by the distribution of recovered meteorites, assuming that the fan-shaped distribution is bilaterally symmetric along the impact trajectory, is along 075° to 085°.

Observations of the Whitecourt crater allow for several impact scenarios that involve the possible atmospheric fragmentation of the incoming meteoroid and the fate of the impactor during impact. The lack of a preserved fusion crust, regmaglypts, or other atmospheric sculpting effects on the bulk of the

meteorites suggest that they spent little or no time traveling through the atmosphere at the velocity required for ablation. We propose that they spalled off the main mass during impact. Additionally, the apparent depth to diameter ratio of the Whitecourt crater (approximately 1:6), similar to that of Meteor Crater, implies that the structure formed as a result of the impact of a single large mass, or near simultaneous impact of a tight swarm of meteorites (Melosh and Collins 2005; Artemieva and Pierazzo 2009). However, this presupposes that the impact was hypervelocity and that the cratering mechanics are similar for the two structures. We conclude that any significant atmospheric fragmentation event must have occurred immediately prior to impact, and that there is a high probability that the impactor traversed the atmosphere without catastrophically fragmenting. High impactor strength, low velocities, and shallow impact angles increase the probability of this occurrence (Schultz 1992c). The lone 6.51 kg sample in Fig. 9C, which must have spalled off the main mass at some higher altitude, suggests that the incoming meteoroid was traveling at a velocity of at least several kilometers per second faster than the 3.0 km s^{-1} limit for ablation at sea level (Allen et al. 1952; Passey and Melosh 1980).

Two scenarios regarding the fate of the impactor are possible for a structure of this scale. In the first scenario, the main body of the impactor is preserved and remains buried in the immediate vicinity of the crater, as would be the case for a penetration crater. This would be similar to many of the smaller craters in the Sikhote Alin crater field (e.g., Krinov 1966). In the second scenario, the impactor is catastrophically disrupted during impact (fragmented, melted, and/or vaporized), as would be the case for an explosively excavated crater formed by a hypervelocity impact. This would be similar to the recent Carancas event (e.g., Tancredi et al. 2009).

Evidence suggests that the incoming meteoroid was catastrophically disrupted during impact. Meteorite fragments spalling off the trailing edge of the impactor once it struck the surface seem the best explanation for the meteorite mass distribution. These spallation products would concentrate down-range and result in the "shrapnel field," or "spall field," observed at the site. The meteorite morphology also appears consistent with impact spallation and is analogous to the proximal meteorites recovered at Meteor Crater, though the Whitecourt samples are not as heavily shocked (e.g., Artemieva and Pierazzo 2009). In addition, the initial magnetic survey results do not reveal the presence of a large buried iron mass near, or below the crater. Further, the presence of small jagged shrapnel, meteorite dust, and Fe-Ni oxide spherules at the base of the transient crater boundary and within the crater fill also strongly suggest impactor disruption and, therefore, that the crater was formed explosively.

Despite our efforts, the evidence of shock we have observed at the Whitecourt crater is limited to the PM observed in quartz grains collected primarily from the fine sand beneath the crater floor, and several Fe-Ni oxide spherules collected from within the crater fill. At present, the impact-origin of these planar features requires further confirmation. In particular, the determination of the orientations of the PM would provide crucial insights into their genesis. The lack of molten target material, rare impactor melt products, and the presence of shrapnel-like meteorites having a well-preserved Widmanstätten pattern suggest that this impact occurred at a velocity lower than the 12–15 km s^{-1} velocities proposed for Meteor Crater (Melosh and Collins 2005; Artemieva and Pierazzo 2009). Based on these observations the impact velocity is likely near the lower limit for an explosively excavated crater and is loosely constrained here as ranging from at least approximately 4 km s^{-1} to approximately 6 km s^{-1}, though could be higher due to the porosity of the target materials. Such low velocities imply that the iron meteoroid entered Earth's atmosphere at an unusually low relative velocity along the proposed trajectory (<10 km s^{-1}). It is unlikely that the meteoroid struck the surface at >10 km s^{-1}.

With the proposed impact angles, velocities, and meteoroid and target material properties it is possible to estimate the radius of the meteoroid at the time of impact. In a manner similar to that of Kenkmann et al. (2009), scaling laws based on the theoretical analysis of cratering mechanics by Holsapple and Schmidt (1987), Housen et al. (1983), and Holsapple (1993—review) are used (1). In particular, the ratio of the final transient crater radius, R, to the radius of the impactor at the time of impact, a, can be determined using the general equation from Holsapple and Housen (2007):

$$\frac{R}{a} = K_1 \left[\frac{ga}{U^2} \left(\frac{\rho}{\delta} \right)^{\frac{2\nu}{\mu}} + \left(\frac{Y}{\rho U^2} \right)^{\frac{2+\mu}{2}} \left(\frac{\rho}{\delta} \right)^{\frac{\nu(2+\mu)}{\mu}} \right]^{\frac{-\mu}{2+\mu}} \quad (1)$$

where K_1, ν, and μ are unit-less scaling coefficients, g is the gravitational acceleration of the target, U is the normal component of the impactor's velocity, ρ is the mass density of the target, δ is the mass density of the impactor, and Y is the cohesive strength of the target material; all values are reported in SI units. Here the impactor is treated as a sphere and the target material as a single unit. The following material properties were used in the calculations: δ = 7,800 kg m^{-3}, R = 14.5 m (the approximate radius of the transient crater as determined using the results of the auger hole data in combination

with the digital elevation map generated using ArcGIS), Y = 1,000 Pa, and ρ = 1,500–2,000 kg m^{-3} (Housen and Holsapple 2003; Holsapple and Housen 2007; Kenkmann et al. 2009). The values for Y and ρ are for dry and water-saturated sand, which are only an approximation of the target materials at the Whitecourt crater. The values for U are obtained from impact velocities between 4 and 6 km s^{-1} for 40° and 55° impact angles. The scaling coefficients are determined experimentally and presently limited to only a few materials. Here we use the values for water-saturated sand (K_1 = 0.93, μ = 0.55, ν = 0.4) and dry sand (K_1 = 1.03, μ = 0.41, ν = 0.4) (Holsapple and Housen 2007). The results of the calculations for both target materials suggest that the impactor was approximately 0.7 m to approximately 1.6 m in diameter (1,285 kg to 16,728 kg) and struck the surface having a kinetic energy of 5 T TNT to 45 T TNT. Determination of the scaling coefficients for the bulk of the target material would allow these values to be refined. Additionally, the target surface consists of two discrete layers, a condition not addressed in this particular model.

In summary, we propose that the Whitecourt crater was formed by a relatively low-energy hypervelocity impact (from approximately 4 km s^{-1} to approximately 6 km s^{-1}) of an approximately 1 m diameter iron impactor traveling along a trend of 060° to 085°, striking the surface at an angle between 40° and 55°. The impactor appears to have transited the atmosphere essentially intact without experiencing catastrophic disruption except possibly immediately prior to striking the surface, resulting in a crater formed from the impact of a tightly bound swarm of meteoroids or single mass. The bulk of the meteorite distribution is therefore the result of spallation during impact.

Acknowledgments— First and foremost, we thank James R. "Sonny" Stevens and Rod Stevens, the individuals who found meteorites at the site and suspected that the unusual depression was an impact crater. For funding we thank the Natural Sciences and Engineering Research Council of Canada (NSERC—PGS-M) and The Barringer Crater Company (the Barringer Family Fund for Meteorite Impact Research) for their awards to R. S. K., Discovery Grant 261740 and Canadian Space Agency (CSA—SSEP CARN) grant to C. D. K. H., and Alberta Ingenuity Funding to D. G. F. The Historic Resources Branch, Alberta Culture and Community Spirit are thanked for permission to carry out research within the protected area. For field assistance we thank Brenton Mah, Marie-Claude Williamson (CSA), Erin Walton, Alberto Reyes, Sasha Blinova, Andy Fagan, Yi Zhao, Rameses D'Souza, and Alister Ling as well as volunteers from the Whitecourt community. For their outstanding work in locating and documenting meteorites at the crater, we thank Murray Paulson's volunteer meteorite hunting team, consisting of Murray Paulson, Brad and Jen Newman, Rick Huziak, Luc and Joan Guillemette, Jake Jakielaszk, Rob Wesel, Mike Bandli, Jason Phillips, and Brian Moore. For assistance in identifying shock effects in quartz and for discussions about impact dynamics, we thank Christian Koeberl (University of Vienna), Peter Schultz and Scott Harris (Brown University), and Jay Melosh (Purdue University). For assistance with materials analysis we thank George Braybrook and De-Ann Rollings (SEM), Sergei Matveev (EMP), and Diane Caird (XRD). Laurence Andriashek (Alberta Geological Survey) is thanked for sharing his knowledge of the regional geology near the crater site. The manuscript benefited from detailed reviews by B. Pratt, G. Tancredi, and R. Herrick.

Editorial Handling—Dr. Nancy Chabot

REFERENCES

Allen W. A., Rinehart J. S., and White W. C. 1952. Phenomena associated with the flight of ultra-speed pellets, part I. Ballistics. *Journal of Applied Physics* 23:132–137.

Artemieva N. and Pierazzo E. 2009. The Canyon Diablo impact event: Projectile motion through the atmosphere. *Meteoritics and Planetary Science* 44:25–42.

Barringer D. M. 1909. *Meteor Crater (formerly called Coon Mountain or Coon Butte), in northern central Arizona*. Read before National Academy of Sciences: Princeton University. Privately Printed.

Brown P., ReVelle D. O., Silber E. A., Edwards W. N., Arrowsmith S., Jackson L. E., Jr., Tancredi G., and Eaton D. 2008. Analysis of a crater-forming impact in Peru. *Journal of Geophysical Research* 113:E09007.

Cassidy W. A., Villar L. M., Bunch T. E., Kohman T. P., and Milton D. J. 1965. Meteorites and craters of Campo del Cielo, Argentina. *Science* 149:1055–1064.

Chen T., Xu H., Xie Q., Chen J., Ji J., and Lu H. 2005. Characteristics and genesis of maghemiite in Chinese loess and paleosols: Mechanism for magnetic susceptibility enhancement in paleosols. *Earth and Planetary Science Letters* 240:790–802.

Demchuk T. D. and Hills L. V. 1991. A re-examination of the Paskapoo Formation in the central Alberta plains: The designation of three new members. *Bulletin of Canadian Petroleum Geology* 39:270–282.

Dietz R. S. 1964. Sudbury structure as an astrobleme. *The Journal of Geology* 72:412–434.

Dominik B. 1976. Mineralogical and chemical study of coarse octahedrite Morasko (Poland). *Prace Mineralogiczne* 47:61.

Fair H. 1987. Hypervelocity then and now. *International Journal of Impact Engineering* 5:1–11.

French B. M. 1998. *Traces of catastophe: a handbook of shockmetamorphic effects in terrestrial meteorite impact structures*. LPI Contribution 954. Houston, Texas: Lunar and Planetary Institute. 120 p.

Gault D. E. and Wedekind J. A. 1978. Experimental studies of oblique impact. Proceedings, 9th Lunar and Planetary Science Conference. pp. 3843–3875.

Gault D. E., Quaide W. L., and Oberbeck V. R. 1965. Interpreting ranger photographs from impact cratering studies. In *The nature of the lunar surface*, edited by Hess W. N., Menzel D. H., and O'Keefe J. A. Baltimore, MD: The Johns Hopkins Press. pp. 125–140.

Grasby S. E., Chen Z., Hamblin A. P., Wozniak P. R., and Sweet A. 2008. Regional characterization of the Paskapoo bedrock aquifer system, southern Alberta. *Canadian Journal of Earth Sciences* 45:1501–1516.

Grieve R. A., Langenhorst F., and Stöffler D. 1996. Shock metamorphism of quartz in nature and experiment: II. Significance in geoscience. *Meteoritics & Planetary Science* 31:6–35.

Gurov E., Gurova E., Chernenko Y., and Yamnichenko A. 2009. The Obolon impact structure, Ukraine, and its ejecta deposits. *Meteoritics & Planetary Science* 44:389–404.

Herd C. D., Froese D. G., Walton E. L., Kofman R. S., Herd E. P., and Duke M. J. 2008. Anatomy of a young impact event in central Alberta: Prospects for the "missing" Holocene impact record. *Geology* 36:955–958.

Herrick R. R. and Forsberg-Taylor N. K. 2003. The shape and appearance of craters formed by oblique impact on the Moon and Venus. *Meteoritics & Planetary Science* 38:1551–1578.

Hodge P. W. 1979. The location of the Haviland meteorite crater. *Meteoritics & Planetary Science* 14:233–234.

Holsapple K. A. 1993. The scaling of impact processes in planetary sciences. *Annual Review of Earth and Planetary Sciences* 21:333–373.

Holsapple K. A. and Housen K. R. 2007. A crater and its ejecta: An interpretation of Deep Impact. *Icarus* 187:345–356.

Holsapple K. A. and Schmidt R. M. 1987. Point source solutions and coupling parameters in cratering mechanics. *Journal of Geophysical Research* 92:6350–6376.

Housen K. R. and Holsapple K. A. 2003. Impact cratering on porous asteroids. *Icarus* 163:102–119.

Housen K., Schmidt R., and Holsapple K. 1983. Crater scaling laws: Fundamental forms based on dimensional analysis. *Journal of Geophysical Research* 88:2485–2499.

Kenkmann T., Artemieva N. A., Wünnemann K., Poelchau M. H., Elbeshausen D., and Núñez del Prado H. 2009. The Carancas meteorite impact crater, Peru: Geologic surveying and modeling of crater formation and atmospheric passage. *Meteoritics & Planetary Science* 44:985–1000.

Koeberl C. 1998. Identification of meteoritic components in impactites. *Geological Society Special Publications* 140:133–153.

Kracher A., Willis J., and Wasson J. T. 1980. Chemical classification of iron meteorites—IX. A new group (IIF), revision of IAB and IIICD, and data on 57 additional irons. *Geochimica et Cosmochimica Acta* 44:773–787.

Krinov E. L. 1966. *Giant meteorites*, 1st English ed. New York: Pergamon Press. 397 p.

Lang B. and Kowalski M. 1973. Sikhote Alin meteoroid: A contribution to the story of its fragmentation and fragment scattering. *Earth and Planetary Science Letters* 21:85–90.

Melosh H. J. 1989. *Impact cratering: A geologic process*. New York: Oxford University Press. 253 p.

Melosh H. J. and Collins G. S. 2005. Meteor Crater formed by low-velocity impact: The paucity of melted rock in this crater may be due to the striking projectile's speed. *Nature* 434:157.

Passey Q. R. and Melosh H. J. 1980. Effects of atmospheric breakup on crater field formation. *Icarus* 42:211–233.

Poag C. W., Powars D. S., Poppe L. J., Mixon R. B., Edwards L. E., Folger D. W., and Bruce S. 1992. Deep sea drilling project site 612 bolide event: New evidence of a Late Eocene impact-wave deposit and a possible impace site, U.S. east coast. *Geology* 20:771–774.

Rasmussen K. L., Aaby B., and Gwozdz R. 2000. The age of the Kaalijärv meteorite craters. *Meteoritics & Planetary Science* 35:1067–1071.

Raukas A., Tiirmaa R., Kaup E., and Kimmel K. 2001. The age of the Ilumetsa meteorite craters in southeast Estonia. *Meteoritics & Planetary Science* 36:1507–1514.

Reinvald I. A. and Luha A. 1928. Bericht über geologische Untersuchungen am Kaalijärv auf Ösel. *Aruanded. Tartu Ülikool Loodusuurijate Selts* 35:30–70.

Robertson P. B. and Grieve R. A. F. 1975. Impact structures in Canada: Their recognition and characteristics. *Journal of the Royal Astronomical Society of Canada* 69:1–21.

Schultz P. H. 1992c. Atmospheric effects on ejecta emplacement and crater formation on Venus from Magellan. *Journal of Geophysical Research* 97:16183–16248.

Scott J. S. 1976. Geology of Canadian tills. In *Glacial till*, edited by Legget R. F. Ottawa: Royal Society of Canada. pp. 50–66.

Shoemaker E. M. and Wynn J. C. 1997. Geology of the Wabar meteorite craters, Saudi Arabia (abstract). 28th Lunar and Planetary Science Conference. pp. 1313–1314.

Soil Classification Working Group. 1998. *The Canadian system of soil classification*, 3rd ed. Ottawa: National Research Council of Canada. 187 p.

Stankowski W. T. 2001. The geology and morphology of the natural reserve "Meteoryt Morasko." *Planetary and Space Science* 49:749–753.

Stankowski W. T., Raukas A., Bluszcz A., and Fedorowicz S. 2007. Luminescence dating of the Morasko (Poland), Kaali, Ilumetsa and Tsoorikmae (Estonia) meteorite craters. *Geochronometria* 28:25–29.

Steiger R. H. and Jager E. 1977. Subcommission on geochronology: Convention of the use of decay constants in geo- and cosmochronology. *Earth and Planetary Science Letters* 36:359–362.

Tancredi G., Ishitsuka J., Schultz P. H., Harris R. S., Brown P., ReVelle D. O., Antier K., Le Pichon A., Rosales D., Vidal E., Varela M. E., Sánchez L., Benavente S., Bojorquez J., Cabezas D., and Dalmau A. 2009. A meteorite crater on Earth formed on September 15, 2007: The Carancas hypervelocity impact. *Meteoritics & Planetary Science* 44:1967–1984.

Tokarsky O. 1977. The hydrogeological reconnaissance maps of Alberta: Map 114. In *Alberta Research Council Bulletin 35—Contributions to the hydrogeology of Alberta*, edited by Toth J. Edmonton: Alberta Research Council Groudwater Division. pp. 1–12.